

1.1 Staging

The decision on whether a regional therapy might induce a benefit for the patient should be based on staging that is as precise as possible. While surgical exploration, palpation, and intraoperative ultrasound have been the gold standard for the detection of distant metastases, the number of patients with small distant metastases in liver, lung, and bone identified by computed tomography, magnetic resonance imaging, and positron emission tomography that cannot be visualized intraoperatively is increasing, reflecting the progress of imaging methods over the last few years (Antoch et al. 2003; Bhattacharjya et al. 2004a). When minimally invasive tumor therapies (MITT) are used, the intervention has to be planned based on imaging alone or combined with a focal exploration such as laparoscopy or video-assisted thoracoscopy. Staging based on imaging alone might induce inappropriate therapy in cases of false-negative or false positive findings, indicating that highly accurate imaging methods are of crucial importance for the planning of image-guided therapies.

On the other hand, the accuracy of imaging methods is still limited for the differentiation of lymphonodal involvement as well as for diffuse tumor infiltrations, i.e., peritoneal carcinomatosis (Antoch et al. 2004). Usually, minimally invasive tumor therapies are used in patients with localized relapse of cancer, involving precise staging where further tumor activity may be excluded by imaging methods. Positron emission tomography using fluorodeoxyglucose (FDG-PET) without or combined with computed tomogra-

phy has been established as the most sensitive imaging modality for the detection of additional tumor manifestations for various types of cancer (Barker et al. 2005; Bipat et al. 2005). Because of the relatively high primary costs and a variable regional availability, only a few patients had PET or PET-CT when they were evaluated for regional tumor therapies. Whole-body MRI has been established during the last 5 years with promising preliminary results for the staging of cancer patients (Blomqvist and Torkzad 2004). Several technical developments have led to the acquisition time for large fields of view being reduced significantly. Whole-body MR imaging protocols can be performed in less than 40 min, making this method attractive for use in daily clinical practice. Whole-body MRI can be combined with organ-specific contrast media such as superparamagnetic iron oxides and hepatobiliary contrast agents with the intention to establish entity-specific protocols in the near future (Semelka and Thermberger 2001). However, there is still a need for systematic and comparative studies for whole-body MRI in oncology. More than 90% of minimally invasive tumor therapies are performed on liver tumors (Gazelle et al. 2000; Bown 1983). Several liver-specific MR contrast media are now established in clinical practice. Reticuloendothelial system-specific agents improve lesion detection by decreasing the signal intensity of background liver on T2-weighted MR images, which increases the conspicuity of focal hepatic lesions with negligible reticuloendothelial cells (e.g., metastases). Hepatocyte-selective agents increase the signal intensity of background liver on T1-weighted images, which

increases the conspicuity of focal lesions that do not contain hepatocytes (e.g., metastases). Several studies have demonstrated a better lesion-based sensitivity of MRI for liver metastases using liver-specific contrast media when compared with CT (Fig. 1.1). However, computed tomography is still the method of choice for the staging of most of the patients in clinical routine because of its versatility (Semelka and Thormberger 2001; Bhattacharjya et al. 2004b). Oncologic CT imaging protocols should include the examination of the liver in several phases, especially when local therapy of liver tumors should be evaluated.

1.2 Image Guidance

For image-guidance of minimal invasive tumor therapies, ultrasound, computed tomography,

and magnetic resonance imaging can be used. Most surgeons and some radiologists, particularly in the United States and Italy, prefer ultrasound (US), while CT is the method of choice for radiologists in several European countries (Gazelle et al. 2000; Tranberg et al. 1994; Vogl et al. 1995; Gaffke et al. 2005).

Ultrasound can be used for image-guided therapies of the liver but cannot be used for interventions of the lung or the bone because of its technical limitations. For image-guided therapies of the liver, ultrasound is widely used because of its good availability, low cost, multiplanarity, and the easiness of handling. Percutaneous use of US for image-guided therapy of the liver is sometimes hampered by reduced image quality due to obesity or inhomogeneous echogenicity of the organ. In addition, the use of US is less favorable for complex image-guided interventions,

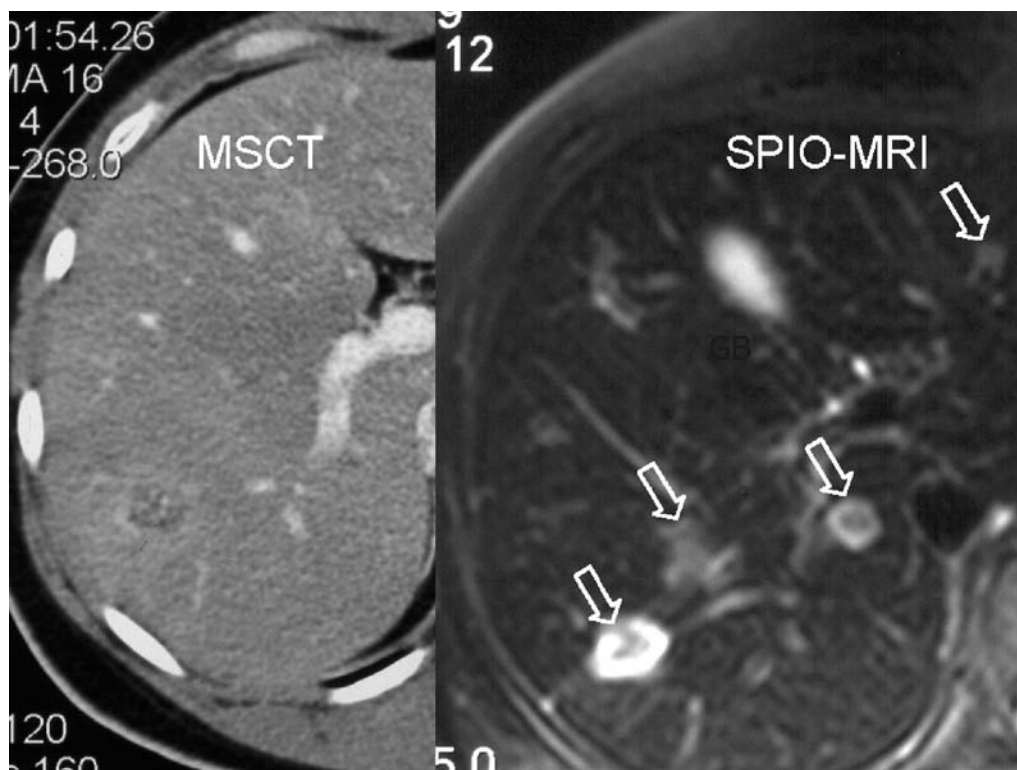


Fig. 1.1 CT and SPIO-MRI of a patient with liver metastases evaluated for minimally invasive tumor therapies. While CT shows poor visualization of liver metastases, MRI using SPIO as liver-specific contrast media demonstrates clearly four hyperintense liver lesions (GB: gallbladder)

i.e., multiapplicator techniques and step-by-step ablations of larger tumors, because of relevant artifacts induced by air that may be brought in during intervention or nitrogen bubbles that occur during thermoablative procedures (Fig. 1.2).

Many radiologists who have access to all imaging modalities prefer CT for image-guided therapy (Vogl et al. 1995; Mahnken et al. 2005; Gaffke et al. 2006). In contrast to ultrasound, both hands can be used for interventional procedures and CT is suitable for intervention in all regions of the body. In addition, complications that may be provoked during intervention such as intra-abdominal bleeding or pneumothoraces can be visualized before clinical signs occur. CT fluoroscopy enabling quasi real-time imaging has been established since the end of the 1990s in many hospitals as being of significant impact for difficult or complex interventions (Fig. 1.3). While diagnostic CT is usually performed with contrast media using arterial, portovenous and venous phases for the detection and differentiation of liver tumors, CT-guided interventions

are performed on plain images. Lesion-based sensitivity of plain CT for liver tumors is poor. In daily clinical practice, the exact position of the applicators must be controlled by contrast-enhanced images during interventions in most cases. In most cases, a sufficient contrast between target lesion and liver tissue can be obtained in a few seconds and repetitive contrast media application is limited by nephrotoxicity. A permanent increase of liver-to-lesion contrast in hepatocellular carcinoma and other hypervascularized tumors can be obtained by intra-arterial application of iodized oil (iodized oil CT, IOCT). However, IOCT has not been established in clinical practice and has its limitation in patients with hypovascular tumors, i.e., liver metastases of most of gastrointestinal tumors and breast tumors (Bhattacharjya et al. 2004a). Because of this limitation, some groups have established a hybrid procedure using CT for the positioning of the applicators in the environment of the tumor and the closed MRI-scanner for multiplanar control of the position, eventually combined

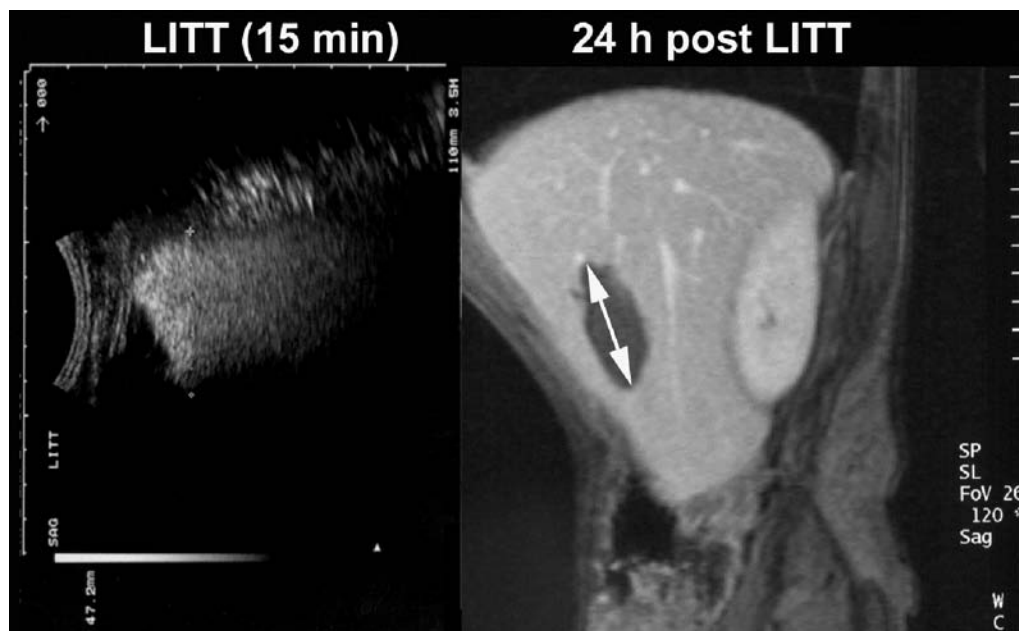


Fig. 1.2 Ultrasound during laser therapy of a liver metastasis and corresponding MRI, both on sagittal orientation. The hyperechogenic area visualized on US is provoked by nitrogen bubbles that occur during tissue heating. US tends to overestimate ablation zone, as demonstrated on postinterventional MRI

with a repositioning in the magnet (Vogl et al. 1995; Gaffke et al. 2006).

Image-guided therapy in closed high-field MRI units is possible (Puls et al. 2003), but time-consuming and often narrowed by the limited space in the MR scanner with a small gantry (Fig. 1.4). Open MRI scanners or MRI with larger gantries enable more comfortable positioning of the applicators (Aschoff et al. 2000). When compared with CT, open MRI seems to be a promising tool for MITT in the nearer future because of the availability of multiplanar near real-time images (MR fluoroscopy) and an optimal, permanent contrast between lesions and normal tissue.

1.3 Thermometry

Until recently, thermoablative therapies were often performed without visual control of the induced temperature. Many factors influence

the size of induced necrosis by thermal ablation techniques (i.e., tissue perfusion, heat conduction) and prevent precise prediction of the size of induced necrosis (Dickinson et al. 1986; Włodarczyk et al. 1998). Some authors used ultrasound to visualize thermal effects during tissue heating. For cryotherapy, excellent visualization of the induced ice ball is possible by ultrasound. In contrast, thermomapping of heated tissue is not possible with ultrasound (Morrison et al. 2000). There is a certain correlation between the appearance of hyperechogenic areas that are provoked by nitrogen bubbles in tissue heated to over 60°C, but these areas do not precisely correlate with the areas where a complete ablation is obtained and may simulate a successful ablation despite incomplete heating (Stroszczyński et al. 2002).

Therefore, several authors use thermosensitive MR sequences for immediate MR temperature monitoring. MR thermometry can be performed precisely using specialized MR sequences in all

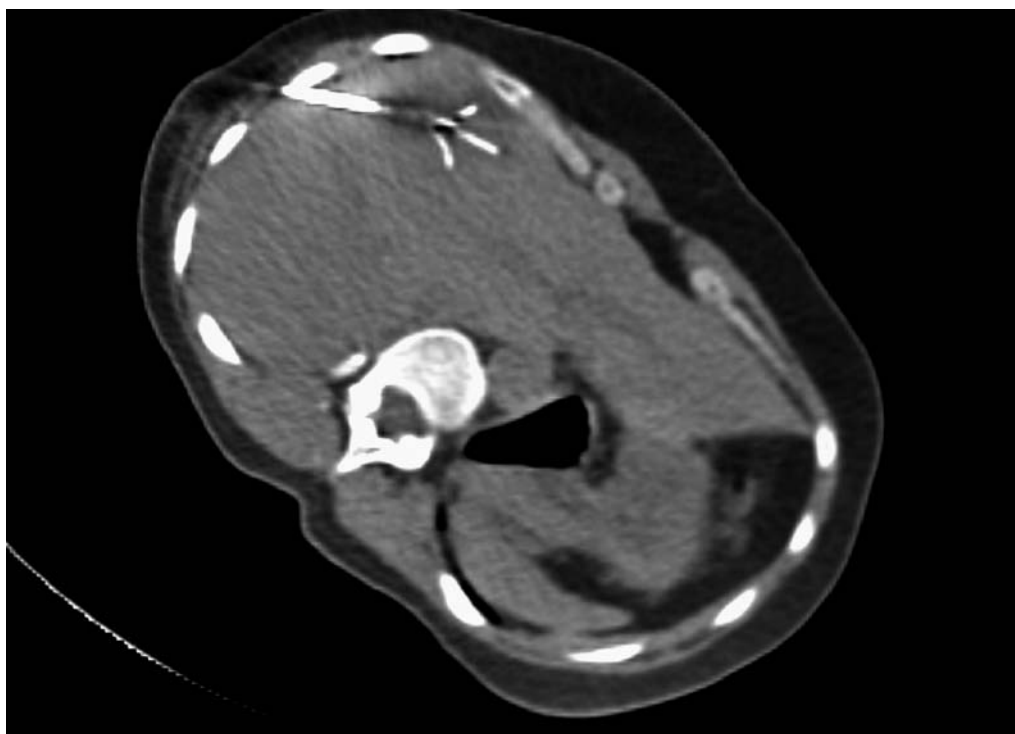


Fig. 1.3 CT fluoroscopy during radiofrequency ablation of a liver tumor

kinds of tissue, i.e., liver, breast, pancreas, and brain (Fig. 1.5) (Matsumoto et al. 1994; Kahn et al. 1998; Olsrud et al. 1998; Stroszczyński et al. 2001). When compared with brain tissue or liver tissue, the temperature monitoring of thermal interventions of the lung is more pretentious because of the susceptibility of surrounding gut and multiple sources of different artifacts. For thermometry, MR-compatible devices are necessary. While laser therapy and cryoablation can be performed during the heating or cooling process, radiofrequency ablation cannot be visualized online because of relevant artifacts induced by the radiofrequency generator. However, sufficient differentiation between devitalized tissue and residual tumor is possible using hyperacute MRI immediately after heating by radiofrequency. In cases of incomplete ablation, the immediate repositioning of the RF device is possible and additional applications may follow (Merkle et al. 1999; Gaffke et al. 2005).

Although proton resonance frequency or dif-

fusion weighted images are more accurate for thermometry in vitro, the T1 method using a FLASH sequence is preferred by several groups because of a high level of robustness (Włodarczyk et al. 1998). Several investigators used temperature-sensitive sequences to reduce the risk of damage of critical structures for thermoablation of liver neoplasms or brain tumors (Gewiese et al. 1994; Kahn et al. 1998).

1.4 Therapy Control

Currently, thermoablative techniques such as laser therapy or radiofrequency ablation are being introduced into clinical practice for the treatment of liver tumors. Based on the analysis of data acquired from liver surgery, a significant impact on survival may be expected in patients with complete tumor ablation only (Scheele and Altendorf-Hofmann 1999). In contrast to surgery, where histopathology enables quality control of



Fig. 1.4 MR-guided radiofrequency ablation of a liver metastasis using a closed high-field scanner. Coronal orientation provides an optimal overview of critical structures such as the costodiaphragmatic angle

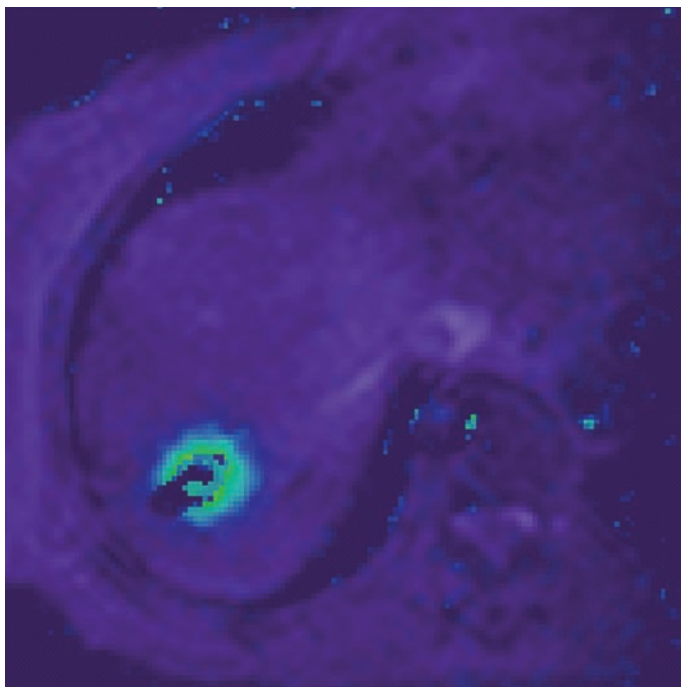


Fig. 1.5 Color-coded temperature mapping during laser therapy of a liver lesion

resection of liver tumors, precise postinterventional imaging is necessary after thermoablative techniques to visualize residual tumor.

To differentiate therapy-induced necrosis from residual tumor, ultrasound, computed tomography, magnetic resonance imaging, and positron emission tomography can be used (Germer et al. 1998; Veit et al. 2006). Therapy-induced necrosis is characterized by low concentrations of water-bounded protons, the absence of blood perfusion, and hypometabolism. In residual tumor tissue, neoangiogenic vessels with capillary leakage induce peripheral edema and cause enhancement of conventional contrast media (Choi et al. 2000). In addition, the tumors show highly proliferative activity and glucose uptake that can be measured by different PET tracers (Veit et al. 2006).

Some groups use MRI for the differentiation between residual tumor and therapy-induced necrosis because of the excellent contrast and spatial resolution in soft tissue (Morrison et al. 1998). Coagulation of tumor or liver tissue leads to tissue drying and results in hypointense lesions on T2-weighted images, while residual

tumor is usually hyperintense caused by tumor edema (Semelka et al. 2000; Stroszczyński et al. 2001). When conventional extracellular contrast media such as Gd-DTPA are used, T1-W images may differentiate between vascularized residual tumor and nonperfused necrosis (Vogl et al. 1995). Liver-specific contrast media such as superparamagnetic iron oxides that enhance in the reticular endothelial system or Gd-EOB or Gd-BOPTA that enhance in healthy hepatocytes may increase contrast between normal liver tissue and thermal-induced necrosis or residual tumor. However, the use of so-called liver specific contrast media does not increase the contrast between residual tumor and thermoablative scar, because liver-specific contrast media only accumulates in healthy liver tissue.

Using healthy animal models, correlations of MRI findings after thermoablation of normal liver tissue on T2-W, plain, and early (0.2- to 10-min) enhanced T1-W images with histopathology were investigated by Germer and Coworkers. Characteristics for complete devitalized liver tissue are hypointensity on T2-W images and the lack of enhancement on early-enhanced (0.2- to

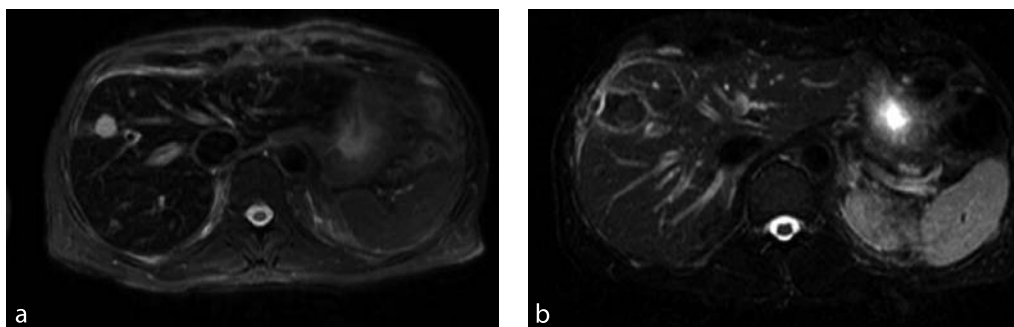


Fig. 1.6 **a** MRI of a patient with solitary liver metastasis of an adenocarcinoma. T2-W images demonstrated a highly hyperintense tumor because of a high concentration of water-bounded protons in the tumor. **b** Five days after radiofrequency ablation, the signal intensity of the tumor and the surrounding tissue is reduced because of coagulation and complete necrosis of the treated area. A small hyperintense rim caused by inflammation around the necrotic area is visible

10-min) T1-W images (Fig. 1.6). In contrast to animal studies, inconclusive or discordant findings on postinterventional MRI are common in clinical practice because of several additional parameters influencing signal intensity of treated areas (i.e., residual tumor, bleeding, injection of fibrin glue and local anesthesia).

Germer et al. systematically correlated MR pattern after i.v. administration of conventional doses of Gd-DTPA (0.1 mmol/kg) of early-enhanced images after LITT of normal livers in 55 rabbits with histomorphologic findings. They observed three zones on MRI and histopathology: the coagulation zone (zone with completely damaged liver tissue), the small transition zone located between the central zone and the undamaged liver tissue, and the reference zone surrounding the lesion with undamaged liver tissue. Early-enhanced MRI correlated well with that obtained macroscopically ($r = 0.96$). Both the central zone and transition zone did not enhance Gd-DTPA 24 h after LITT on early-enhanced images. However, the transition zone reflecting a zone where residual tumor cells may be found measured approximately 2 mm and may be neglected in clinical practice. In contrast to findings of Aschoff and co-workers, lesions of patients with complete ablation were significantly larger on T2-W images on this study, indicating the limited value of this sequence for early postinterventional control.

Late-enhanced MRI 10 min to 6 h after administration of extracellular contrast media

(Gd-DTPA) is considered as to be specific for necrotic tissue, i.e., for myocardial infarction (Ni et al. 2001) and could be used for imaging of necrotic areas. Mechanisms of delayed enhancement in devitalized tissue have remained unclear until now. Similar to the hypothesis concerning the uptake of metalloporphyrins, active protein binding of the macrocyclic extracellular Gd complexes in the transition zone with or without consecutive alteration of T1-relaxivity could be a possible cause for delayed enhancement. These findings might be of importance for early postinterventional therapy planning.

Recently, positron emission tomography (PET) without or combined with computed tomography (PET/CT) using [F-18] fluorodeoxyglucose (FDG) has been investigated for the evaluation of liver metastases after radiofrequency ablation and other interstitial tumor therapies. FDG PET and PET/CT can provide added diagnostic information compared with conventional imaging in patients after radiofrequency ablation of liver metastases and can be useful in guiding repeat ablation procedures (Veit et al. 2006). PET/CT therefore possibly proved superior to CT alone when assessing the liver for residual tumor after RFA. However, false-negative results may occur using PET/CT hidden by normal FDG-uptake in surrounding normal liver tissue. The most sensitive approach detecting residual disease in liver treated by minimally invasive tumor therapies seems to be a combined use of MRI and FDG-PET. While PET-MRI scanners

have not been available until now, retrospective fusion of MRI and PET data can be easily done based on commercially available software tools. The most important supplementary finding supplied by image fusion is a more precise correlation with focal tracer hot spots in PET (Fig. 1.7).

References

1. Antoch G, Vogt FM, Freudenberg LS, Nazaradeh F, Goehde SC, Barkhausen J, Dahmen G, Bockisch A, Debatin JF, Ruehm SG (2003) Whole-body dual-modality PET/CT and whole-body MRI for tumor staging in oncology. *JAMA* 290:3199–3206

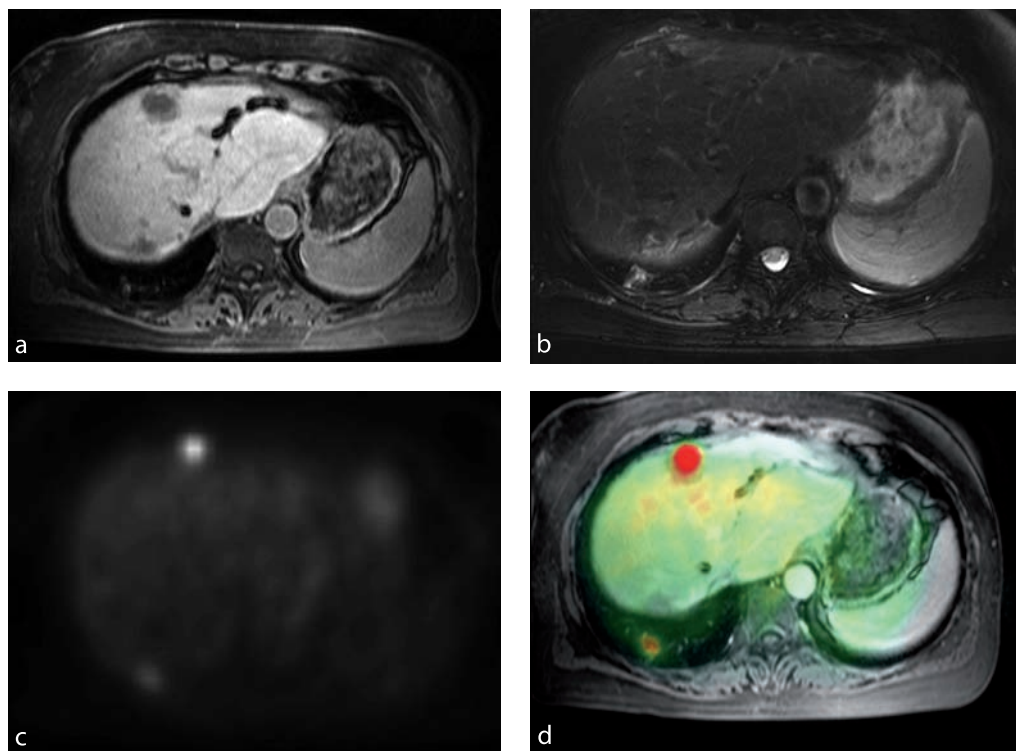


Fig. 7 a Contrast-enhanced MRI of a patient with colorectal cancer and hemihepatectomy. Two new liver metastases were treated by radiofrequency ablation (RFA) 6 months ago. MRI was performed because of rising CEA level during follow-up. Contrast enhanced T1-W images demonstrate two hypointense scars after RFA. b On T2-W images, a hyperintense area close to the ventral scar is visualized, suggesting local recurrence. In addition, a hyperintense focal lung lesion is visible. c FDG-PET on axial orientation shows two hypermetabolic areas, both suggesting tumor activity. It remains unclear if the second focus is located in the lung or in the liver (Courtesy of Dr. Dresel, Chairman of the Dept. of Nuclear Medicine Robert-Rössle Klinik Charité Campus Buch). d Fusion of FDG-PET and MRI underlines local recurrence in the ventral liver lesion and the appearance of the new lung metastases. In contrast, no activity is visualized in the second liver lesion

2. Antoch G, Saoudi N, Kuehl H, Dahmen G, Mueller SP, Beyer T, Bockisch A, Debatin JF, Freudenberger LS (2004) Accuracy of whole-body dual-modality fluorine-18-2-fluoro-2-deoxy-D-glucose positron emission tomography and computed tomography (FDG-PET/CT) for tumor staging in solid tumors: comparison with CT and PET. *J Clin Oncol* 22:4357–4368
3. Aschoff AJ, Rafie N, Jesberger JA et al. (2000) Thermal lesion conspicuity following interstitial radiofrequency thermal tumor ablation in humans: a comparison of STIR, turbo spin-echo T2-weighted, and contrast-enhanced T1-weighted MR images at 0.2 T. *J Magn Reson Imaging* 12:584–589
4. Barker DW, Zagoria RJ, Morton KA, Kavanagh PV, Shen P (2005) Evaluation of liver metastases after radiofrequency ablation: utility of 18F-FDG PET and PET/CT. *Am J Roentgenol* 184:1096–1102
5. Bhattacharjya S, Bhattacharjya T, Baber S, Tibballs JM, Watkinson AF, Davidson BR (2004a) Prospective study of contrast-enhanced computed tomography, computed tomography during arteriography, and magnetic resonance imaging for staging colorectal liver metastases for liver resection. *Br J Surg* 91:1361–1369
6. Bhattacharjya S, Bhattacharjya T, Quaglia A, Dhillon AP, Burroughs AK, Patch DW, Tibballs JM, Watkinson AF, Rolles K, Davidson BR (2004b) Liver transplantation in cirrhotic patients with small hepatocellular carcinoma: an analysis of pre-operative imaging, explant histology and prognostic histologic indicators. *Dig Surg* 21:152–159
7. Bipat S, van Leeuwen MS, Comans EF, Pijl ME, Bossuyt PM, Zwinderman AH, Stoker J (2005) Colorectal liver metastases: CT, MR imaging, and PET for diagnosis-meta-analysis. *Radiology* 237:123–131
8. Blomqvist L, Torkzad MR (2004) Whole-body imaging with MRI or PET/CT: the future for single-modality imaging in oncology? *JAMA* 290:3248–3249
9. Bown SG (1983) Phototherapy of tumors. *World J Surg* 7:700–709
10. Choi SI, Jiang CZ, Lim KH et al. (2000) Application of breath-hold T2-weighted, first-pass perfusion and gadolinium-enhanced T1-weighted MR imaging for assessment of myocardial viability in a pig model. *J Magn Reson Imaging* 11:476–480
11. Dickinson RJ, Hall AS, Hind AJ, Young IR (1986) Measurement of changes in tissue temperature using MR imaging. *J Comp Assist Tomogr* 10:468–472
12. Gaffke G, Gebauer B, Gnauck M, Knollmann F, Helmberger T, Ricke J, Oettle H, Felix R, Stroszczynski C (2005) Potential advantages of the MRI for the radiofrequency ablation of liver tumors. *Fortschr Rontgenstr* 177:77–84
13. Gaffke G, Gebauer B, Knollmann FD, Helmberger T, Ricke J, Oettle H, Felix R, Stroszczynski C (2006) Use of semiflexible applicators for radiofrequency ablation of liver tumors. *Cardiovasc Intervent Radiol* 29:270–275
14. Gazelle GS, Goldberg SN, Solbiati L, Livraghi T (2000) Tumor ablation with radio-frequency energy. *Radiology* 217:633–646
15. Germer CT, Isbert CM, Albrecht D et al. (1998) Laser-induced thermotherapy for the treatment of liver metastasis: correlation of gadolinium-DTPA-enhanced MRI with histomorphologic findings to determine criteria for follow-up monitoring. *Surg Endosc* 12:1317–1325
16. Gewiese B, Beuthan J, Fobbe F, Stiller D, Mueller G, Boese-Landgraf J, Wolf KJ, Deimling M (1994) Magnetic resonance imaging-controlled laser-induced interstitial thermotherapy. *Invest Radiol* 29:345–351
17. Kahn T, Harth T, Kiwit JC, Schwarzmaier HJ, Wald C, Modder U (1998) In vivo MRI thermometry using a phase-sensitive sequence: preliminary experience during MRI-guided laser-induced interstitial thermotherapy of brain tumors. *J Magn Reson Imaging* 8:160–164
18. Mahnken AH, Rohde D, Brkovic D, Gunther RW, Tacke JA (2005). Percutaneous radiofrequency ablation of renal cell carcinoma: preliminary results. *Acta Radiol* 46:208–214
19. Matsumoto R, Mulkern RY, Hushek SG, Jolesz FA (1994) Tissue temperature monitoring for thermal interventional therapy: comparison of T1-weighted MR sequences. *J Magn Reson Imaging* 4:65–70
20. Merkle EM, Haaga JR, Duerk JL, Jacobs GH, Brambs HJ, Lewin JS (1999) MR imaging-guided radio-frequency thermal ablation in the pancreas in a porcine model with a modified clinical C-arm system. *Radiology* 213:461–467

21. Morrison PR, Jolesz FA, Charous D et al. (1998) MRI of laser-induced interstitial thermal injury in an in vivo animal liver model with histologic correlation. *J Magn Reson Imaging* 18:57–63
22. Ni Y, Pislaru C, Bosmans H et al. (2001) Intracoronary delivery of Gd-DTPA and Gadophrin-2 for determination of myocardial viability with MR imaging. *Eur Radiol* 11:876–883
23. Olsrud J, Wirestam R, Brockstedt S, Nilsson AM, Tranberg KG, Stahlberg F, Persson BR (1998) MRI thermometry in phantoms by use of the proton resonance frequency shift method: application to interstitial laser thermotherapy. *Phys Med Biol* 43:2597–2613
24. Puls R, Stroszczynski C, Gaffke G, Hosten N, Felix R, Speck U (2003) Laser-induced thermotherapy (LITT) of liver metastases: MR-guided percutaneous insertion of an MRI-compatible irrigated microcatheter system using a closed high-field unit. *J Magn Reson Imaging* 17:663–670
25. Scheele J, Altendorf-Hofmann A (1999) Resection of colorectal liver metastases. *Langenbecks Arch Surg* 384:313–327
26. Semelka RC, Helmberger TK (2001) Contrast agents for MR imaging of the liver. *Radiology* 218:27–38
27. Semelka RC, Hussain SM, Marcos HB, Woosley JT (2000) Perilesional enhancement of hepatic metastases: correlation between MR imaging and histopathologic findings: initial observations. *Radiology* 215:89–94
28. Silverman SG, Tuncali K, Adams DF, vanSonnenberg E, Zou KH, Kacher DF, Morrison PR, Jolesz FA (2000) MR imaging-guided percutaneous cryotherapy of liver tumors: initial experience. *Radiology* 217:657–664
29. Stroszczynski C, Hosten N, Puls R, Nagel S, Scholman HJ, Wlodarczyk W, Oettle H, Moesta KT, Schlag PM, Felix R (2001) Histopathological correlation to MRI findings during and after laser-induced thermotherapy in a pig pancreas model. *Invest Radiol* 36:413–421
30. Stroszczynski C, Gretschel S, Gaffke G, Puls R, Kretzschmar A, Hosten N, Schlag PM, Felix R (2002) Laser-induced thermotherapy (LITT) for malignant liver tumours: the role of sonography in catheter placement and observation of the therapeutic procedure (in German). *Ultraschall Med* 23:163–167
31. Tranberg KG, Moller PH, Hannesson P, Stenram U (1994) Percutaneous interstitial laser hyperthermia in clinical use. *Ann Chir Gynaecol* 83:286–290
32. Veit P, Antoch G, Stergar H, Bockisch A, Forsting M, Kuehl H (2006) Detection of residual tumor after radiofrequency ablation of liver metastasis with dual-modality PET/CT: initial results. *Eur Radiol* 16:80–87
33. Vogl TJ, Muller PK, Hammerstingl R, Weinhold N, Mack MG, Philipp C, Deimling M, Beuthan J, Pegios W, Riess H et al. (1995) Malignant liver tumors treated with MR imaging-guided laser-induced thermotherapy: technique and prospective results. *Radiology* 196:257–265
34. Wlodarczyk W, Boroschewski R, Hentschel M, Wust P, Monich G, Felix R (1998) Three-dimensional monitoring of small temperature changes for therapeutic hyperthermia using MR. *J Magn Reson Imaging* 8:165–174



<http://www.springer.com/978-3-540-28137-5>

Minimally Invasive Tumor Therapies

Stroszczyński, C. (Ed.)

2006, VII, 146 p.,

ISBN: 978-3-540-28137-5